ACCSCIENCE PUBLISHING

Microbes & Immunity

ORIGINAL RESEARCH ARTICLE

Intracellular *Fusobacterium nucleatum* attenuates poly(ADP-ribose) polymerase inhibitor-induced cGAS–STING signaling in head and neck squamous cell carcinoma cells

Negar Taghavi Pourianazar*

Medical Laboratory Techniques Program, Vocational School of Health Services, Istanbul Aydin University, Istanbul, Turkey

Abstract

Head and neck squamous cell carcinoma (HNSCC) harbors one of the densest intratumoral microbiomes of any solid tumor, yet it is unknown whether resident oral bacteria interfere with the innate immune signaling underlying poly(ADP-ribose) polymerase inhibitor (PARPi) efficacy. This study examined the effect of *Fusobacterium nucleatum* colonization on olaparib-induced DNA damage signaling, cyclic GMP–AMP synthase (cGAS)–stimulator of interferon genes (STING)–type I interferon (IFN) activation, and innate immune crosstalk in HSC3 and SCC25 HNSCC cell lines. Oxidative DNA damage was measured by 8-hydroxy-2′-deoxyguanosine competitive enzyme-linked immunosorbent assay (ELISA); cGAS–STING, checkpoint (*CD274*), and tolerogenic (*TGFB1*) transcripts by quantitative reverse transcription polymerase chain reaction; and cytokine secretion, including macrophage activation in conditioned-media transfer assays, by sandwich ELISA. Olaparib induced dose-dependent oxidative DNA damage, cytotoxicity (IC_{50} ≈ 5.6 μM in HSC3 and 7.9 μM in SCC25), and robust cGAS–STING activation, increasing *IFNB1* expression 8–11-fold and IFN-β secretion 6–9-fold. Co-culture with live *F. nucleatum* did not acutely compromise tumor cell fitness but attenuated olaparib-induced IFN-β and C-X-C motif chemokine ligand 10 secretion by 55%–70% and upregulated *CD274* and *TGFB1*. Macrophage tumor necrosis factor alpha release provoked by conditioned media from bacteria-free, olaparib-treated cells (3.4-fold) was reduced by more than 60% when tumor cells carried intracellular bacteria, and direct STING agonism partially restored interferon output. *F. nucleatum* thus dampens PARPi-elicited cGAS–STING innate immune signaling and skews the tumor secretome toward immune evasion, providing a rationale for combining PARPi with STING agonists or microbiome-directed interventions in HNSCC.

Keywords: *Fusobacterium nucleatum*; Poly(ADP-ribose) polymerase inhibitor; Olaparib; cGAS–STING; Type I interferon; Head and neck squamous cell carcinoma; Tumor microbiome; Innate immunity

***Corresponding author:**
Negar Taghavi Pourianazar
(Negarpourianazar@aydin.edu.tr)

Citation: Taghavi Pourianazar N. Intracellular *Fusobacterium nucleatum* attenuates poly(ADP-ribose) polymerase inhibitor-induced cGAS–STING signaling in head and neck squamous cell carcinoma cells. *Microbes & Immunity*.
doi: 10.36922/MI026340104

Received: August 21, 2026

Revised: October 3, 2026

Accepted: October 9, 2026

Published online: October 30, 2026

Copyright: © 2026 Author(s). This is an Open-Access article distributed under the terms of the Creative Commons Attribution License, permitting distribution, and reproduction in any medium, provided the original work is properly cited.

Publisher's Note: AccScience Publishing remains neutral with regard to jurisdictional claims in published maps and institutional affiliations.

1. Introduction

Head and neck squamous cell carcinoma (HNSCC) is the sixth most common malignancy worldwide and remains one of the most immunologically complex solid tumors. Beyond the well-established roles of human papillomavirus (HPV) infection, tobacco, and alcohol, the local microbial ecosystem of the upper aerodigestive tract is increasingly recognized as a determinant of tumor initiation, progression, and treatment response.[1,2] The oral cavity hosts more than 700 bacterial species, and recent culture-independent surveys have demonstrated that HNSCC tissue is not sterile but contains an intratumoral microbiome that is compositionally distinct from adjacent normal mucosa.[3,4] Longitudinal epidemiological data further indicate that oral microbial dysbiosis precedes and predicts HNSCC risk, implicating the microbiota in disease development rather than mere passenger colonization.[5,6]

Among oral commensals-turned-pathogens, *Fusobacterium nucleatum* occupies a central position. This anaerobic, Gram-negative bacterium is a keystone species of periodontal biofilms and is consistently enriched in oral and oropharyngeal tumor tissue.[7,8] *F. nucleatum* contributes to oncogenesis through multiple mechanisms, including the activation of β-catenin signaling via *Fusobacterium* adhesin A, the recruitment of pro-tumorigenic myeloid cells, and, critically, the active suppression of local antitumor immunity.[9,10] The outer-membrane protein Fap2 engages the inhibitory receptor T cell immunoreceptor with Ig and ITIM domains (TIGIT) on natural killer (NK) cells and T lymphocytes, while RadD and other surface proteins induce lymphocyte apoptosis, establishing a permissive immune niche.[10,11] In HNSCC specifically, intratumoral *Fusobacterium* colonization has been associated with elevated programmed death-ligand 1 (PD-L1) expression and reduced response to immune checkpoint blockade,[12,13] and intracellular bacteria at the invasive front carry prognostic implications.[14] Very recent work in *Nature Cancer* demonstrated that intratumoral bacteria are broadly immunosuppressive and promote immunotherapy resistance in HNSCC.[15]

Paralleling these microbiological advances, poly(ADP-ribose) polymerase inhibitors (PARPi) have attracted substantial interest in HNSCC.[16,17] Clinical PARPi trap PARP1 and PARP2 on damaged DNA, converting repairable lesions into cytotoxic lesions and driving cell death through replication fork collapse.[18] Importantly, the therapeutic value of PARPi extends beyond cytotoxicity: PARP inhibition induces replication fork collapse and the accumulation of cytosolic double-stranded DNA fragments, which engage the cyclic GMP–AMP synthase (cGAS)–stimulator of interferon genes (STING)–TANK-binding kinase 1 (TBK1)–interferon regulatory factor 3 (IRF3) pathway and drive type I interferon production, thereby "resetting" the inflammatory tumor microenvironment and sensitizing tumors to immune checkpoint blockade.[19-21] Shen *et al.*[20] showed that this STING-dependent immune activation occurs independently of *BRCA* status—a finding of particular relevance to HNSCC, which is not classically *BRCA*ness-driven—while Moutafi *et al.*[16,17] have translated the PARPi immune-resetting rationale into phase II window trials of olaparib alone or with cisplatin or durvalumab in operable HNSCC, and a subsequent phase II trial combining olaparib with pembrolizumab and carboplatin reported encouraging synergy between PARPi and anti-programmed cell death protein 1 (PD-1) therapy.[22]

Two research streams—the immunobiology of intratumoral bacteria and the immunomodulatory pharmacology of PARPi—have thus matured largely in parallel. Yet one fundamental question remains unaddressed: does the intratumoral microbiome modulate the innate immune signaling that underlies PARPi efficacy? This question is biologically plausible and clinically urgent. Oral bacteria persist within HNSCC cells, and tumor-infiltrating immune cells,[15,23] bacterial nucleases, cyclic dinucleotides, and metabolites can all intersect with cytosolic DNA sensing and interferon signaling.[24,25] Previous work showed that reactive oxygen species (ROS)-induced DNA damage enhances sensitivity to PARP inhibition in HSC3 and SCC25 HNSCC cell lines.[26] This finding prompted evaluation of whether microbial colonization could conversely tune this DNA damage-dependent immunogenic axis.

In the present study, two HNSCC cell lines, HSC3 and SCC25, were co-cultured with live *F. nucleatum*, heat-killed bacteria, or cell-free bacterial supernatant to assess the consequences of bacterial colonization for olaparib-induced oxidative DNA damage, cGAS–STING signaling, type I interferon and chemokine secretion, and the activation of innate immune cells in conditioned-media transfer assays. It is hypothesized that intracellular *F. nucleatum* attenuates PARPi-triggered innate immune signaling and biases the tumor secretome toward immune evasion, thereby attenuating the immunological benefits of PARP inhibition.

2. Materials and methods

2.1. Reagents and materials

Olaparib (≥99% purity) was purchased from Selleckchem (United States). The STING agonists 2'3'-cGAMP and diABZI STING agonist 1 were obtained from Sigma-Aldrich (United States) and MedChemExpress (United

States), respectively. Dulbecco's modified Eagle medium, RPMI 1640, fetal bovine serum (FBS), L-glutamine, and penicillin–streptomycin were obtained from Gibco (Thermo Fisher Scientific, United States). Phorbol 12-myristate 13-acetate, gentamicin sulfate, Triton X-100, dimethyl sulfoxide (DMSO), methanol, crystal violet, hemin, and menadione were obtained from Sigma-Aldrich (United States). The 3-(4,5-dimethylthiazol-2-yl)-2,5-diphenyltetrazolium bromide (MTS) assay (cat. no.: G3580) was purchased from Promega (United States). Brain–heart infusion (BHI) broth and blood agar plates were from Oxoid (Thermo Fisher Scientific, United Kingdom). TRIzol reagent and the SYBR Green quantitative polymerase chain reaction (PCR) master mix (cat. no.: 4309155) were from Thermo Fisher Scientific (United States); the RNeasy Mini Kit (cat. no.: 74104) and RNase-free DNase I were purchased from Qiagen (Germany). Human interferon beta (IFN-β; cat. no.: 41410-1), C-X-C motif chemokine ligand 10 (CXCL10)/interferon gamma-induced protein 10 (IP-10; cat. no.: DIP100), tumor necrosis factor alpha (TNF-α; cat. no.: DTA00D), and interleukin-6 (IL-6; D6050B) sandwich enzyme-linked immunosorbent assay (ELISA) kits were obtained from R&D Systems (Bio-Techne, United States), and the 8-hydroxy-2'-deoxyguanosine (8-OHdG) competitive ELISA Kit (cat. no.: 501130) was purchased from Cayman Chemical (United States).

2.2. Cell lines and culture conditions

The human oral squamous cell carcinoma (OSCC) cell lines HSC3 (derived from a gingival primary tumor) and SCC25 (derived from a tongue primary tumor), THP-1 human monocytic cells, and immortalized human oral keratinocytes, OKF6/TERT-1, used as the non-malignant oral epithelial comparator, were kindly provided by Professor Dr. Omer Faruk Bayrak, Department of Medical Genetics, Faculty of Medicine, Yeditepe University (Istanbul, Turkey). HSC3 was selected because it is an HPV-negative, well-characterized OSCC line derived from the gingiva, an oral subsite consistently reported to harbor dense intratumoral bacterial communities[7,15]—and because previous work established it as a reliable model of ROS-dependent DNA damage signaling in response to PARP inhibition[26]; SCC25 was included as a tongue-derived counterpart to ensure that the findings were not restricted to a single anatomical subsite or cell line-specific artifact. HSC3 and SCC25 cells were maintained in Dulbecco's modified Eagle medium supplemented with 10% FBS, 1% penicillin–streptomycin, and 2 mM L-glutamine at 37 °C in a humidified atmosphere containing 5% carbon dioxide. THP-1 cells were cultured in RPMI 1640 with 10% FBS and differentiated into macrophage-like cells by treating them with 100 ng/mL phorbol 12-myristate 13-acetate for 48 h, followed by 24 h of rest in fresh medium before use in conditioned-media experiments. All cell lines were routinely screened for mycoplasma contamination prior to experimental use, and all experiments were performed with mycoplasma-negative cells maintained exclusively between passages 5 and 20 throughout the study to minimize passage-related phenotypic drift.

2.3. Bacterial strains and culture conditions

Fusobacterium nucleatum subsp. *nucleatum* was cultivated in BHI broth supplemented with hemin (5 μg/mL) and menadione (1 μg/mL) (Sigma-Aldrich, United States) in an anaerobic chamber (85% N_2, 10% H_2, 5% CO_2) at 37 °C. Bacteria were harvested in mid-logarithmic phase, washed three times with sterile phosphate-buffered saline (PBS), and resuspended at defined densities. For heat-killed controls, bacterial suspensions were incubated at 95 °C for 20 min, and killing was confirmed by the absence of growth on blood agar plates after 72 h of anaerobic incubation. Bacterial supernatant was obtained by centrifuging overnight anaerobic cultures at 12,000× *g* for 20 min and filtering the clarified supernatant (0.22 μm), which was then stored at −80 °C until use.

2.4. Co-culture of head and neck squamous cell carcinoma cells with *Fusobacterium nucleatum*

Head and neck squamous cell carcinoma cells were seeded in 6-well plates (or 96-well plates for viability assays) and allowed to adhere for 24 h. For infection, bacteria were added at multiplicities of infection (MOI) of 1, 10, 50, and 100 and co-incubated for 2, 6, and 24 h under anaerobic conditions. After the indicated periods, extracellular bacteria were removed by washing three times with PBS supplemented with 100 μg/mL gentamicin (Sigma-Aldrich, United States), followed by two PBS washes, thereby retaining primarily cell-associated and intracellular bacteria. Parallel conditions received an equal volume of filtered bacterial supernatant or heat-killed bacteria with equivalent bacterial protein content. Heat-killed bacteria were therefore used as a control for bacterial components rather than as a direct comparison for bacterial internalization. Intracellular bacterial loads were quantified by lysing tumor cells in 0.1% Triton X-100, performing ten-fold serial dilutions, and plating on blood agar; colony-forming units (CFU) were counted after 72 h of anaerobic incubation.

2.5. Drug treatments

Olaparib was dissolved in DMSO at 100 mM and stored at −20 °C; working dilutions were prepared in complete medium immediately before use, with a final DMSO concentration not exceeding 0.1% (vehicle controls

received equivalent DMSO). Cells were treated with 0.5, 1, 2, 5, 10, and 20 μM olaparib for 24, 48, and 72 h. In bacterial co-culture experiments, olaparib was added 24 h after the gentamicin-protection washing step and maintained for 48 h. For pathway-stimulation experiments, the STING agonist 2'3'-cGAMP (5 μg/mL) or the non-nucleotidyl STING agonist diABZI (1 μM) was added during the final 24 h of treatment where indicated.

2.6. Cell viability assay

Cell viability was determined by the MTS assay. Cells seeded in 96-well plates (4×10^3 cells/well) were treated as described, and 20 μL of 5 mg/mL MTS solution was added for four hours. Formazan crystals were dissolved in DMSO, and absorbance was measured at 570 nm (reference 630 nm) on a microplate reader. Half-maximal inhibitory concentrations (IC_{50}) were calculated from dose–response curves fitted to a four-parameter logistic model.

2.7. Oxidative DNA damage assay

Oxidative DNA damage was quantified by measuring 8-OHdG, a well-established biomarker of oxidative guanine lesions. Following treatment, HSC3, SCC25, and OKF6/TERT-1 cells were harvested, and genomic DNA was extracted with the QIAamp DNA Mini Kit (cat. no.: 51304, Qiagen, Germany) according to the manufacturer's instructions. DNA was enzymatically digested to nucleosides, and 8-OHdG was quantified using a competitive ELISA kit, in which 8-OHdG in the sample competes with a tracer-conjugated 8-OHdG for binding to a fixed amount of anti-8-OHdG antibody; signal intensity is inversely proportional to sample 8-OHdG concentration. Results were expressed as pg 8-OHdG per μg of genomic DNA, using a standard curve generated in each run, with all samples assayed in duplicate.

2.8. RNA extraction and quantitative reverse transcription polymerase chain reaction

Total RNA was extracted with TRIzol reagent, purified with the RNeasy Mini Kit, treated with DNase I, and quantified spectrophotometrically. Complementary DNA was synthesized from 1 μg of total RNA using oligo(dT) primers and SuperScript IV reverse transcriptase (Thermo Fisher Scientific). Quantitative PCR was performed in SYBR Green master mix on a QuantStudio 5 real-time thermal cycler (Applied Biosystems, United States) with the following cycling conditions: 95 °C for 10 min, followed by 40 cycles of 95 °C for 15 s and 60 °C for 1 min. Primer sequences targeting *GAPDH* (housekeeping), *CGAS*, *TMEM173* (STING), *TBK1*, *IRF3*, *IFNB1*, *CXCL10*, *IL6*, *TNF*, *CD274* (PD-L1), and *TGFB1* are provided in Table 1. Melting curve analysis confirmed amplification specificity, and relative expression was calculated by the $2^{-\Delta\Delta Ct}$ method, normalized to *GAPDH* and the corresponding untreated control condition.

2.9. Enzyme-linked immunosorbent assays

Human IFN-β, CXCL10/IP-10, TNF-α, and IL-6 concentrations in cell culture supernatants were measured using commercial sandwich ELISA kits according to the manufacturers' instructions. For tumor-cell secretome analyses, conditioned media were collected after 48 h of treatment, clarified by centrifugation (1,000× *g*, 5 min) to remove detached cells, and aliquoted for storage at −80 °C. In macrophage crosstalk experiments, THP-1-derived macrophages (2×10^4 cells/well in 24-well plates) were exposed to conditioned media from HNSCC treatments diluted 1:2 in fresh RPMI 1640 with 5% FBS for 24 h, and TNF-α and IL-6 released into the supernatant were quantified by ELISA. All samples were assayed in duplicate, with standard curves generated in each run.

2.10. Statistical analysis

All experiments were performed in at least three independent biological replicates, each with two to four technical replicates. Data are expressed as mean ± standard deviation unless otherwise indicated. Comparisons between two groups were performed with unpaired Student's *t*-tests, while comparisons across multiple groups used one-way or two-way analysis of variance followed by Tukey's post hoc test, as appropriate. Log-transformed CFU counts were analyzed with mixed-effects models to account for plate-level clustering. A two-sided p-value < 0.05 was considered statistically significant. Analyses were performed with GraphPad Prism 8 (GraphPad Software, United States).

3. Results

3.1. *Fusobacterium nucleatum* infects and persists within HSC3 and SCC25 cells without acute cytotoxicity

To first establish that *F. nucleatum* can form a stable association with HNSCC cells under the co-culture conditions used throughout the study, HSC3 and SCC25 monolayers were exposed to live bacteria at MOI 1–100 for 2–24 h, and cell-associated bacterial loads were quantified after gentamicin protection. Both cell lines supported bacterial association in a dose- and time-dependent manner. In HSC3 cells, association increased from 420 ± 90 CFU/well at MOI 10 (2 h) to 310,000 ± 60,000 CFU/well at MOI 100 (24 h); SCC25 cells showed a comparable but consistently lower trajectory (280 ± 70 to 190,000 ± 50,000 CFU/well), consistent with previously reported cell

Table 1. Primer sequences used for quantitative reverse transcription polymerase chain reaction

Gene	Primer direction	Sequence (5'–3')	Product length (bp)	Tm (°C)
CGAS	Forward	TGGAGTCTGCGAATGATGCT	138	60.0
	Reverse	CTGCTCTCCACATCGTCCAG		60.1
TMEM173	Forward	CTGCTCATGGTGCTGAAGCT	145	59.9
	Reverse	GCAGGTTGTCCTTGTCTCCA		60.0
TBK1	Forward	GCAAGCTGTGGAGTTCATCG	133	60.1
	Reverse	CTCAGCACCCACTTTGTCCT		60.0
IRF3	Forward	AGCTGCAGGATGACGACTCA	141	59.8
	Reverse	CCTTCCTGCTTGTCTGGTCT		60.0
IFNB1	Forward	CCCAAGGAGATCTTCAGCAAT	124	60.0
	Reverse	TCTGCTCTGCTTGGTGATTC		60.1
CXCL10	Forward	GCTGATGCAGCCACCGTG	130	60.2
	Reverse	ATGTTCTGATGCCATCTCTGAT		59.9
IL6	Forward	CTTTCCAGAGAGACATTCAAGCC	127	60.0
	Reverse	TGGCTGCTTCTTTCTGATTCC		60.1
TNF	Forward	CTCCTCTCCATCCTCCAGAT	144	59.9
	Reverse	CCAAGGACAGCCTCTCCTCA		60.0
CD274	Forward	GCTACAGAGGGTCTATGCAGC	136	60.0
	Reverse	CATTGCTGGTCACACCTTTC		60.1
TGFB1	Forward	AGCGACCATCCATGACATG	148	59.9
	Reverse	GATGTTGTTGCCCAGTACC		60.0
GAPDH	Forward	ATGGGGAAGGTGAAGGTCG	121	59.5
	Reverse	GGGGTCATTGATGGCAACAATA		59.3

line-specific differences in *Fusobacterium* uptake. Heat-killed bacteria were included as a control for bacterial components and were normalized to the live bacterial preparations using equivalent total bacterial protein content. Because they were nonviable, their cell association and internalization were not quantified by CFU, and no direct imaging-based assay was performed. Cell-free bacterial supernatant, by definition, yielded no CFU after gentamicin washing and served as an acellular stimulus control.

Importantly, bacterial association did not acutely compromise tumor cell fitness. MTS assays performed 24 h after infection showed that HSC3 and SCC25 viability remained at 93–101% of uninfected controls across all MOI and bacterial preparations tested, indicating that the co-culture system models chronic intracellular colonization rather than overt bacterial cytotoxicity. This stable colonization window, previously established in oral bacteria–OSCC co-culture systems,[27] was therefore used for all downstream functional experiments (Figure 1).

3.2. Olaparib induces dose-dependent oxidative DNA damage and cytotoxicity in head and neck squamous cell carcinoma cell lines

Consistent with previous evidence that ROS-induced DNA damage sensitizes these cell lines to PARP inhibition,[26] olaparib produced concentration-dependent cytotoxicity in both HNSCC cell lines (Figure 2A). After 48 h of exposure, HSC3 viability reduced to 78% ± 5%, 52% ± 6%, and 21% ± 4% at 2, 5, and 10 μM, respectively, yielding an IC_{50} of 5.6 ± 0.7 μM; SCC25 cells were modestly more resistant, with a viability of 84% ± 4%, 61% ± 5%, and 31% ± 5% at the same concentrations (IC_{50} 7.9 ± 0.9 μM). In contrast, normal OKF6/TERT-1 keratinocytes showed only a marginal decline across the same concentration range (96% ± 3% at 2 μM, 94% ± 3% at 5 μM, and 91% ± 3% at 10 μM), retaining 83% ± 4% viability even at 20 μM, so that no IC_{50} was reached within the tested window (> 20 μM). This ~4-fold separation between the IC_{50} values of the tumor lines and the surviving fraction of normal keratinocytes establishes a therapeutically meaningful selectivity window for the dose range used in the subsequent experiments.

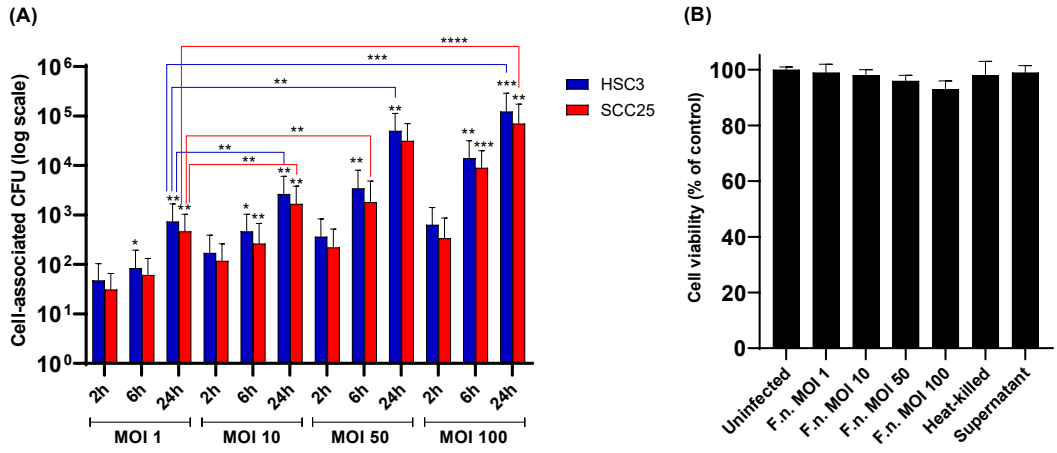


Figure 1. *Fusobacterium nucleatum* (F.n.) associates with HNSCC cells in a dose-dependent manner without acute cytotoxicity. (A) Cell-associated CFU of HSC3 and SCC25 at MOI 1–100 after co-culture, plotted on a logarithmic scale. For each cell line separately, within each MOI, the 6- and 24-h values were compared with the corresponding 2-h value. At 24 h, values at MOI 10, 50, and 100 were compared with MOI 1. (B) MTS viability of infected, heat-killed, and supernatant-treated cells relative to uninfected controls at 24 h. Data are mean ± SD ($n = 3$). Statistical significance: *$p < 0.05$, **$p < 0.01$, ***$p < 0.001$, ****$p < 0.0001$ compared to control.

Abbreviations: CFU: Colony-forming units; HNSCC: Head and neck squamous cell carcinoma; MOI: Multiplicity of infection; MTS: 3-(4,5-dimethylthiazol-2-yl)-2,5-diphenyltetrazolium bromide; SD: Standard deviation.

The 8-OHdG competitive ELISA confirmed that this cytotoxicity was accompanied by accumulation of oxidative DNA lesions, a principal intermediate of PARP trapping-induced replication stress. In HSC3 cells, genomic 8-OHdG rose in a dose-dependent manner from a vehicle baseline of 4.2 ± 0.7 pg/μg DNA to 11.3 ± 1.6, 24.7 ± 2.9, and 38.5 ± 3.4 pg/μg at 2, 5, and 10 μM olaparib, respectively (Figure 2B). SCC25 cells mounted a closely similar response (4.5 ± 0.8 to 35.8 ± 3.2 pg/μg across the same concentrations), consistent with their comparable sensitivity in the viability assay. OKF6/TERT-1 cells, by contrast, accumulated only a modest lesion burden (6.1 ± 0.9 and 9.4 ± 1.2 pg/μg at 5 and 10 μM, respectively, reaching 12.8 ± 1.5 pg/μg only at 10 μM), consistent with their markedly preserved viability. Because sustained PARP trapping and unrepaired oxidative lesion accumulation are established mechanisms of PARPi cytotoxicity, these data collectively establish that both tumor lines, but not normal keratinocytes, mount a robust dose-dependent oxidative DNA damage response to olaparib, providing the lesion substrate for innate immune sensing in the subsequent experiments (Figure 2).

3.3. Olaparib activates the cGAS–STING pathway and induces type I interferon secretion in head and neck squamous cell carcinoma cells

An examination was subsequently conducted to determine whether olaparib-induced DNA damage engages the cytosolic DNA sensing machinery in these oral cancer cell lines, mirroring reports in breast, ovarian, and lung cancer models.[19-21] In axenic culture, 48-h treatment with 5 μM olaparib increased CGAS and *TMEM173* (STING) transcript levels 2.1–2.6-fold in both lines, while downstream transcripts were induced more strongly: *IFNB1* increased 9.4 ± 1.6-fold in *HSC3* and 7.8 ± 1.3-fold in *SCC25*, and *CXCL10* increased 14.2 ± 2.4-fold and 11.6 ± 1.9-fold, respectively. *IRF3* transcripts showed a modest 1.6-fold increase, consistent with post-translational rather than transcriptional regulation of this factor.

At the protein secretion level, IFN-β concentrations in conditioned media rose from below the detection limit of the assay in vehicle controls to 38 ± 7 pg/mL in HSC3 (Figure 3B) and 29 ± 6 pg/mL in SCC25 (Figure 3C) after 48 h of 5 μM olaparib; CXCL10 increased from 0.9 ± 0.3 ng/mL to 5.4 ± 0.8 ng/mL (HSC3) and from 0.8 ± 0.2 ng/mL to 4.6 ± 0.7 ng/mL (SCC25). The response scaled with drug concentration up to 10 μM and was accompanied by a smaller but significant rise in proinflammatory IL-6 (2.3-fold) and TNF (1.8-fold) transcripts. These results demonstrate that, in the absence of microbial interference, PARP inhibition functions as a potent activator of the cGAS–STING–type I interferon axis in oral squamous carcinoma cells, extending the immunomodulatory paradigm described by Shen *et al.*[20], Ding *et al.*[21], and Lee *et al.*[28] to the HNSCC context (Figure 3).

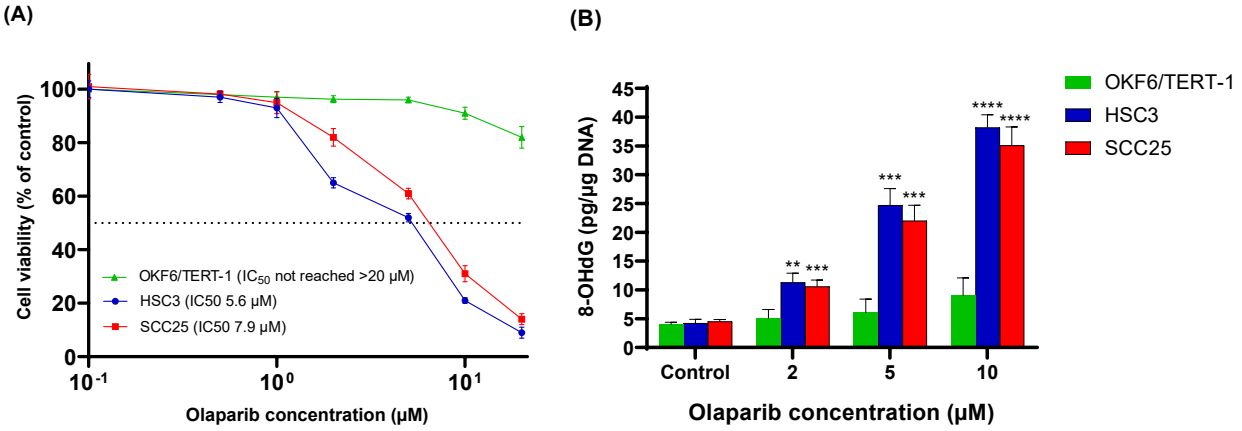


Figure 2. Olaparib induces dose-dependent oxidative DNA damage and cytotoxicity in HNSCC cells. (A) MTS dose–response curves after 48 h of treatment in HSC3, SCC25, and OKF6/TERT-1 cells (mean ± SD, $n = 3$); dashed line indicates 50% viability; the IC_{50} for OKF6/TERT-1 was not reached above 20 μM. (B) 8-OHdG competitive ELISA quantification of oxidative DNA damage in HSC3, SCC25, and OKF6/TERT-1 cells after 48 h of treatment. Data are presented as mean ± SD ($n = 3$). For pairwise comparisons between adjacent olaparib doses, one-way ANOVA followed by Tukey's post-hoc test was used. $^{**}p<0.01$, $^{***}p<0.001$, $^{****}p<0.0001$.

Abbreviations: ANOVA: Analysis of variance; ELISA: Enzyme-linked immunosorbent assay; HNSCC: Head and neck squamous cell carcinoma; 8-OHdG: 8-Hydroxy-2'-deoxyguanosine; IC_{50}: Half-maximal inhibitory concentration; MTS: 3-(4,5-dimethylthiazol-2-yl)-2,5-diphenyltetrazolium bromide; SD: Standard deviation.

3.4. Intracellular *Fusobacterium nucleatum* suppresses poly(ADP-ribose) polymerase inhibitor-induced innate immune signaling and upregulates immune checkpoint and tolerogenic transcripts

When HSC3 and SCC25 cells were co-cultured with live *F. nucleatum* (MOI 10–100, 24-h association followed by 48 h of combined culture), the olaparib-induced transcriptional program was markedly blunted. At MOI 100, 5 μM olaparib reduced *IFNB1* induction from 9.4-fold to 3.1-fold in HSC3 and from 7.8-fold to 2.6-fold in SCC25 (compared with infected, untreated cells); *CXCL10* induction fell from 14.2-fold to 4.9-fold and from 11.6-fold to 4.1-fold. STING pathway transcripts were likewise suppressed, with *CGAS* and *TMEM173* induction falling to near baseline (1.1–1.3-fold versus 2.1–2.6-fold in bacteria-free cells). Secreted IFN-β showed corresponding reductions of 62% in HSC3 (38 ± 7 versus 14 ± 4 pg/mL) and 62% in SCC25 (29 ± 6 versus 11 ± 3 pg/mL), and CXCL10 decreased by 68% in HSC3 (5.4 ± 0.8 versus 1.7 ± 0.4 ng/mL) and 67% in SCC25 (4.6 ± 0.7 versus 1.5 ± 0.3 ng/mL) (Figure 4). Notably, the olaparib-induced rise in 8-OHdG was not significantly altered by bacterial colonization (38.5 ± 3.4 versus 36.9 ± 3.7 pg/μg in infected HSC3 cells), indicating that *F. nucleatum* interferes downstream of lesion formation, at the level of damage sensing or signaling rather than DNA damage itself.

Concomitantly, bacterial colonization shifted the transcriptome toward immune evasion. *CD274* (PD-L1) expression rose 2.8 ± 0.4-fold in infected HSC3 and 2.4 ± 0.3-fold in infected SCC25 relative to uninfected treated controls, while *TGFB1* increased 2.6-fold and 2.1-fold; *IL6* transcripts, in contrast, were elevated approximately 3-fold, reflecting a mixed but overall tolerogenic profile. Heat-killed bacteria produced partial suppression (approximately 30%–40% reduction in IFN-β release versus 62%–68% for live bacteria), and cell-free supernatant exerted only minor effects (10%–15% reduction), indicating that viable, cell-associated *F. nucleatum*—rather than soluble bacterial products alone—is required for full attenuation of the PARPi-induced innate response (Figures 4 and 5).

3.5. *Fusobacterium nucleatum* colonization dampens innate immune cell activation in conditioned-media transfer assays

To assess the functional immunological consequence of these secretome changes, THP-1-derived macrophages were exposed to conditioned media collected from the four key conditions: untreated cells, olaparib-treated cells, *F. nucleatum*-infected cells, and infected cells treated with olaparib. Conditioned media from olaparib-treated, bacteria-free HNSCC cells provoked a robust macrophage activation phenotype, increasing TNF-α release 3.4-fold (from 210 ± 38 to 712 ± 84 pg/mL) and IL-6 release 2.9-fold relative to media from untreated cells. This activation was attributable to the enriched IFN-β and CXCL10 content of PARPi-conditioned media, consistent with the known priming effect of type I interferon on mononuclear phagocytes.[28,29]

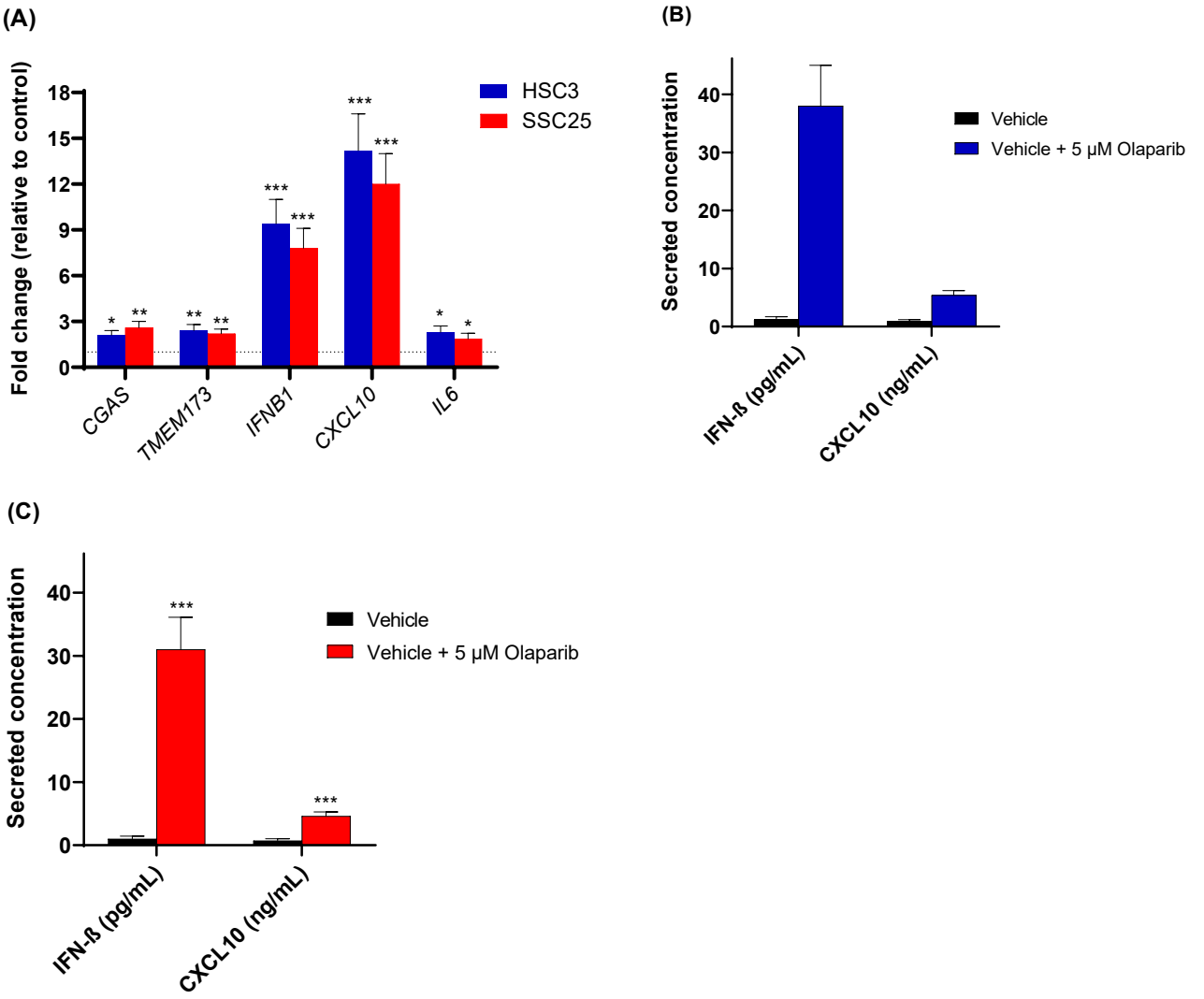


Figure 3. Olaparib activates the cGAS–STING pathway and type I interferon secretion in axenic HNSCC culture. (A) qRT-PCR fold induction of *CGAS*, *TMEM173* (STING), *IFNB1*, *CXCL10*, and *IL6* after 48 h of 5 µM olaparib in HSC3 and SCC25 cells (vehicle reference at 1.0-fold, dashed line). (B) ELISA quantification of IFN-β and CXCL10 in conditioned media of HSC3 cells and (C) SCC25 cells (B, C: mean ± SD, $n = 3$; *$p < 0.05$, **$p < 0.01$, ***$p < 0.001$ versus the respective vehicle control, unpaired t-test).

Abbreviations: cGAS: Cyclic GMP–AMP synthase; CXCL10: C-X-C motif chemokine ligand 10; ELISA: Enzyme-linked immunosorbent assay; HNSCC: Head and neck squamous cell carcinoma; IFN-β: Interferon beta; qRT-PCR: Quantitative reverse transcription polymerase chain reaction; SD: Standard deviation; STING: Stimulator of interferon genes.

Intracellular *F. nucleatum* abrogated this crosstalk. Macrophages exposed to conditioned media from infected, olaparib-treated cells released only 264 ± 41 pg/mL TNF-α and 178 ± 27 pg/mL IL-6 in HSC3 (reductions of 63% and 59% relative to the bacteria-free PARPi condition) and 242 ± 38 pg/mL TNF-α and 163 ± 24 pg/mL IL-6 in SCC25 (reductions of 62% and 65%)—responses indistinguishable from those elicited by media from untreated cells. Notably, bacterial colonization alone (without olaparib) also reduced basal macrophage activation relative to control media (TNF-α 138 ± 25 pg/mL), suggesting that *F. nucleatum* imposes both a constitutive suppressive tone and an active blockade of damage-induced immune stimulation. Together, these data indicate that intracellular *F. nucleatum* uncouples PARPi-induced DNA damage from functional innate immune engagement in the tumor microenvironment (Figure 6).

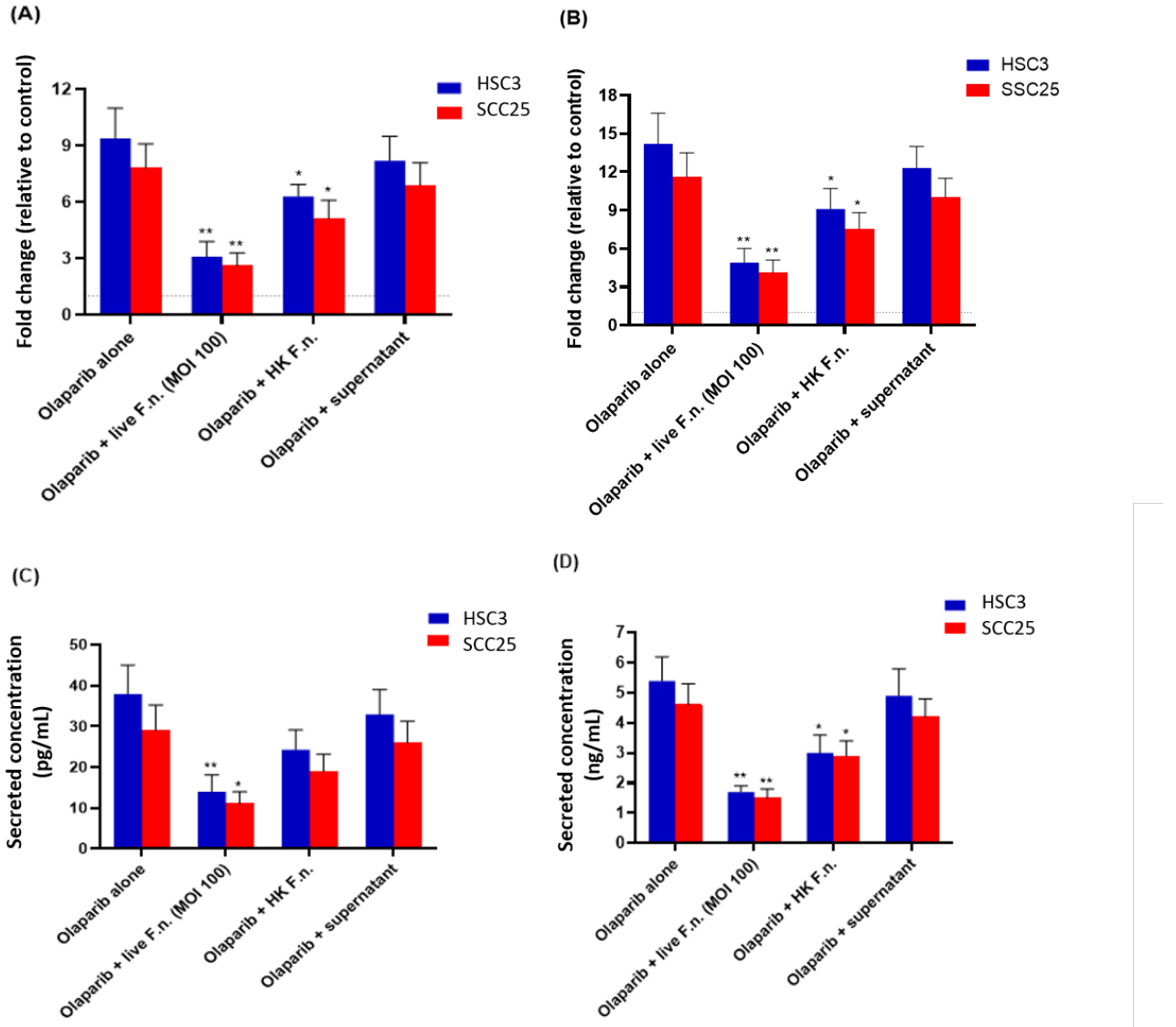


Figure 4. Live intracellular *Fusobacterium nucleatum* (F.n.) suppresses PARPi-induced innate immune signaling. HSC3 and SCC25 cells were treated with olaparib (5 μM, 48 h) alone or in combination with live *F. nucleatum* (MOI 100), heat-killed bacteria, or cell-free bacterial supernatant. (A) *IFNB1* induction measured by qRT-PCR: olaparib alone 9.4 ± 1.6-fold (HSC3) and 7.8 ± 1.3-fold (SCC25), reduced to 3.1 ± 0.8-fold and 2.6 ± 0.7-fold by live bacteria. (B) CXCL10 induction measured by qRT-PCR: olaparib alone 14.2 ± 2.4-fold (HSC3) and 11.6 ± 1.9-fold (SCC25), reduced to 4.9 ± 1.1-fold and 4.1 ± 0.9-fold by live bacteria. (C) IFN-β secretion measured by ELISA (pg/mL): olaparib alone 38 ± 7 (HSC3) and 29 ± 6 (SCC25), reduced to 14 ± 4 and 11 ± 3 by live bacteria. (D) CXCL10 secretion measured by ELISA (ng/mL): olaparib alone 5.4 ± 0.8 (HSC3) and 4.6 ± 0.7 (SCC25), reduced to 1.7 ± 0.4 and 1.5 ± 0.3 by live bacteria. Data are mean ± SD ($n = 3$; $^{*}p < 0.05$, $^{**}p < 0.01$ versus olaparib alone for each cell line; heat-killed bacteria showed partial suppression, supernatant minimal effect).

Abbreviations: CXCL10: C-X-C motif chemokine ligand 10; ELISA: Enzyme-linked immunosorbent assay; HNSCC: Head and neck squamous cell carcinoma; IFN-β: Interferon beta; MOI: Multiplicity of infection; PARPi: Poly(ADP-ribose) polymerase inhibitor; qRT-PCR: Quantitative reverse transcription polymerase chain reaction; SD: Standard deviation.

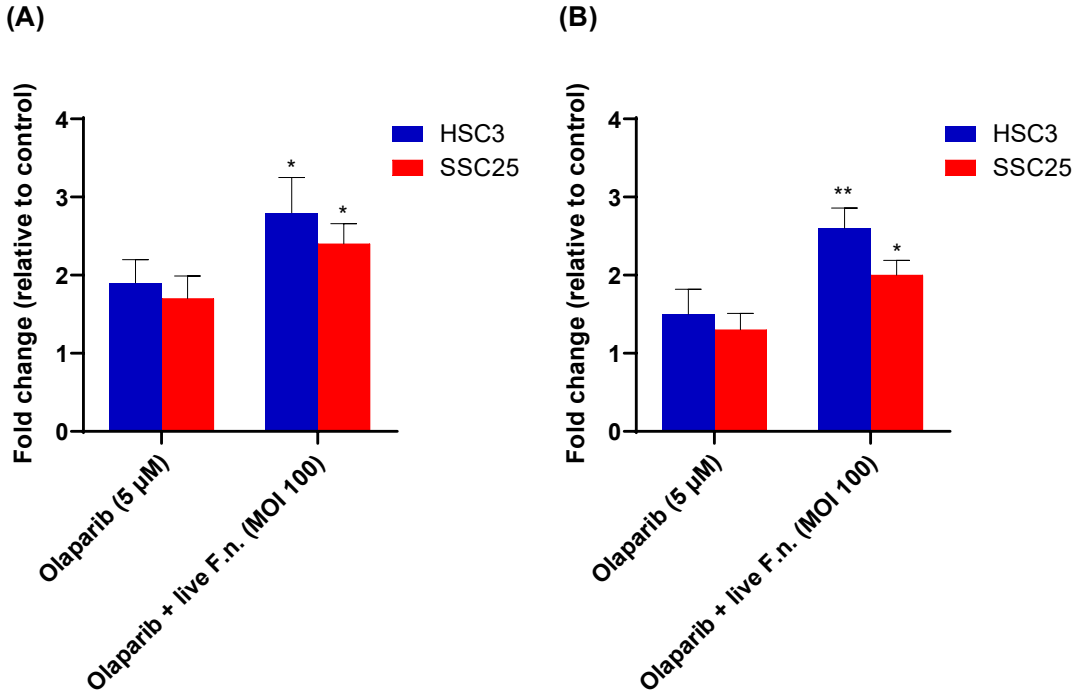


Figure 5. Bacterial colonization upregulates immune evasion transcripts. Fold changes of (A) *CD274* (PD-L1) and (B) *TGFB1* (TGF-β1) in HSC3 and SCC25 cells treated with olaparib (5 μM) alone or in combination with live *Fusobacterium nucleatum* (F.n.) (MOI 100) for 48 h. Data are mean ± SD (n = 3; *$p < 0.05$, **$p < 0.01$ versus olaparib alone for each cell line).
Abbreviations: MOI: Multiplicity of infection; PD-L1: Programmed death-ligand 1; SD: Standard deviation; TGF-β1: Transforming growth factor beta 1.

3.6. Direct STING stimulation partially restores innate immune signaling in infected, poly(ADP-ribose) polymerase inhibitor-treated cells

An investigation was conducted to determine if the suppressive effect of *F. nucleatum* could be overcome by bypassing the attenuated upstream sensing step. Co-administration of the STING agonist 2'3;-cGAMP (5 μg/mL) or diABZI (1 μM) during the final 24 h of olaparib treatment restored *IFNB1* induction to 7.1-fold in HSC3 and 5.9-fold in SCC25 (versus 3.1-fold and 2.6-fold with olaparib alone in infected cells) and recovered IFN-β secretion to approximately 70% of the level achieved in bacteria-free, olaparib-treated cells. *CD274* upregulation was not reversed by STING agonism (2.7-fold), indicating that some bacterial effects operate independently of the cGAS–STING node, whereas the chemokine defect—*CXCL10* restoration to 9.4-fold—was largely corrected. These pharmacological rescue data localize the principal site of microbial interference to innate DNA sensing rather than to terminal interferon effector function, and they support the therapeutic logic of combining PARPi with direct STING agonism in microbe-colonized HNSCC (Figure 7).

4. Discussion

The principal finding of this study is that intracellular *F. nucleatum* colonization of HNSCC cells selectively blunts the cGAS–STING–type I interferon axis activated by PARPi-induced DNA damage, suppresses the secretion of the immune-attractant chemokine CXCL10, upregulates the immune checkpoint ligand PD-L1 and the tolerogenic cytokine TGF-β1, and thereby weakens the capacity of the tumor secretome to activate innate immune cells. These results bridge two research areas that have hitherto advanced in parallel—the immunobiology of the intratumoral microbiome and the immunomodulatory pharmacology of PARPi—and provide the first direct evidence that an intratumoral oral pathogen can interfere with PARPi-induced innate immune signaling in head and neck cancer cells (Figure 8).

Olaparib activates robust cGAS–STING signaling in oral squamous carcinoma lines, extending the

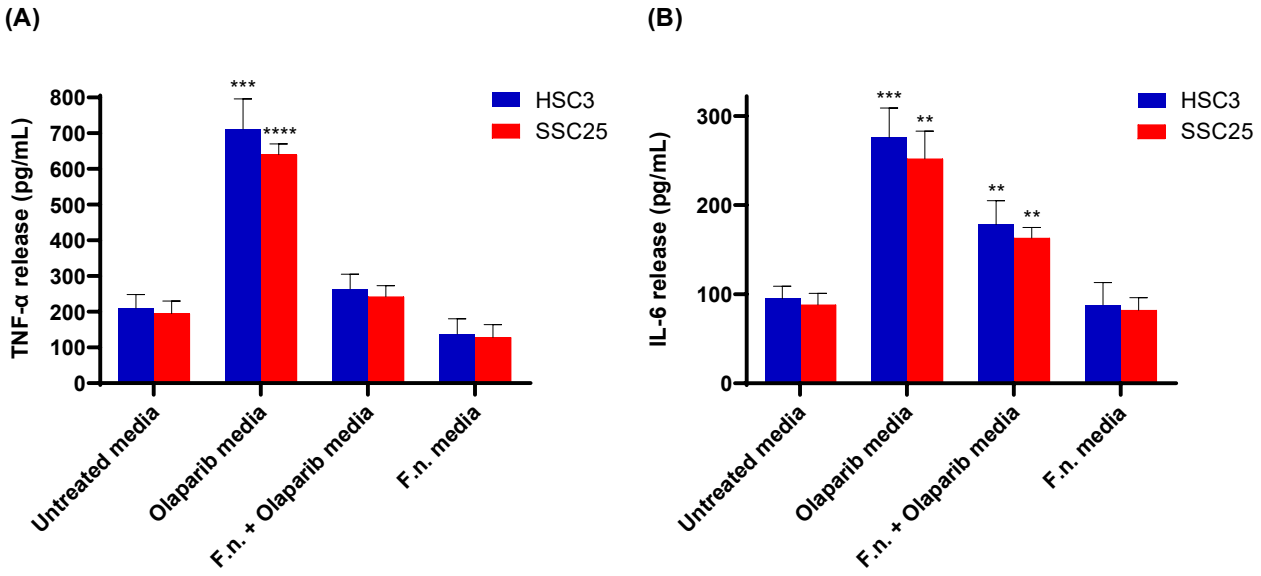


Figure 6. *Fusobacterium nucleatum* (F.n.) dampens innate immune crosstalk between conditioned media and THP-1-derived macrophages. (A) TNF-α release (pg/mL) by THP-1-derived macrophages after 24 h of exposure to conditioned media from untreated, olaparib-treated (5 μM, 48 h), *F. nucleatum*-infected plus olaparib-treated, or bacteria-only conditions, in HSC3 and SCC25 cells. (B) IL-6 release (pg/mL) under the same conditions. Data are mean ± SD ($n = 3$; $^{**}p < 0.01$, $^{***}p < 0.001$, and $^{****}p < 0.0001$ versus untreated media for each cell line).
Abbreviations: IL-6: Interleukin 6; SD: Standard deviation; TNF-α: Tumor necrosis factor alpha.

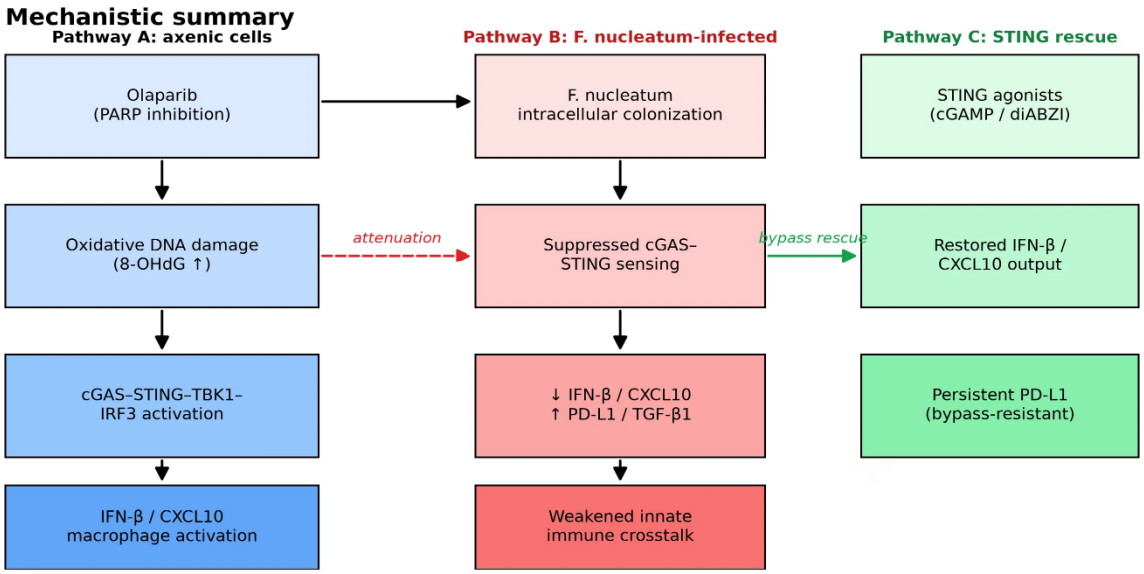


Figure 7. Mechanistic summary. Pathway A: In axenic HNSCC cells, olaparib-induced oxidative DNA damage engages cGAS–STING signaling and drives IFN-β/CXCL10 secretion and macrophage activation. Pathway B: Intracellular *F. nucleatum* attenuates cGAS–STING sensing, reducing interferon output, elevating PD-L1/TGF-β1, and weakening innate immune crosstalk. Pathway C: Direct STING agonism bypasses the microbial block to partially restore interferon and chemokine signaling, though PD-L1 upregulation persists.
Abbreviations: cGAMP: Cyclic GMP–AMP; cGAS: Cyclic GMP–AMP synthase; CXCL10: C-X-C motif chemokine ligand 10; 8-OHdG: 8-Hydroxy-2'-deoxyguanosine; IFN-β: Interferon beta; PARP: Poly(ADP-ribose) polymerase; PD-L1: Programmed death-ligand 1; STING: Stimulator of interferon genes; TBK1: TANK-binding kinase 1; TGF-β1: Transforming growth factor beta 1; IRF3: Interferon regulatory factor 3.

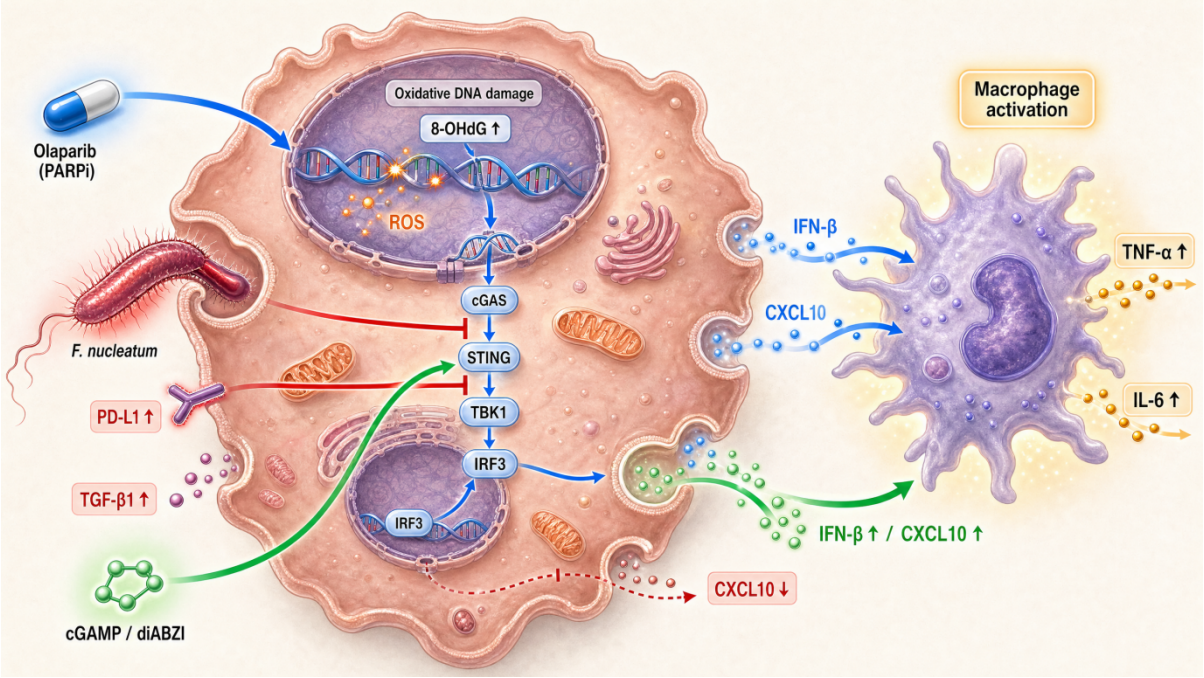


Figure 8. Proposed mechanism by which intracellular *F. nucleatum* attenuates PARPi-induced cGAS–STING signaling in HNSCC cells. Blue pathway (activation): Olaparib induces oxidative DNA damage (8-OHdG accumulation, ROS), cytosolic DNA engages the cGAS–STING–TBK1–IRF3 cascade, and the resulting IFN-β/CXCL10 secretion primes macrophage activation with elevated TNF-α and IL-6 release. Red pathway (suppression): *F. nucleatum* blocks the cGAS–STING–TBK1 axis, blunts chemokine output, and upregulates PD-L1 and TGF-β1, shifting the tumor cell toward an immunosuppressive phenotype. Green pathway (rescue): Direct STING stimulation with cGAMP or diABZI bypasses the microbial block and partially restores interferon and chemokine secretion. Created using Nano Banana Pro (Taghavi Pourianazar N.), 2026.
Abbreviations: cGAMP: Cyclic GMP–AMP; cGAS: Cyclic GMP–AMP synthase; CXCL10: C-X-C motif chemokine ligand 10; 8-OHdG: 8-Hydroxy-2'-deoxyguanosine; IFN-β: Interferon beta; PARP: Poly(ADP-ribose) polymerase; PD-L1: Programmed death-ligand 1; ROS: Reactive oxygen species; STING: Stimulator of interferon genes; TBK1: TANK-binding kinase 1; TGF-β1: Transforming growth factor beta 1; IRF3: Interferon regulatory factor 3.

immunomodulatory paradigm established in other tumor types. Shen *et al.*[20] demonstrated that PARPi trigger the accumulation of cytosolic double-stranded DNA and consequent activation of the cGAS–STING–TBK1–IRF3 cascade, inducing type I interferon and sensitizing tumors to checkpoint blockade independently of BRCA status; Ding *et al.*[21] showed that olaparib elicits local and systemic STING-dependent antitumor immunity involving both innate and adaptive compartments in *Brca1*-mutant ovarian cancer models; and Pantelidou *et al.*[19] established that PARPi efficacy depends on $CD8^+$ T-cell recruitment via intratumoral STING activation in triple-negative breast cancer models. Lee and Konstantinopoulos[28] have comprehensively reviewed how PARP inhibition reshapes both innate and adaptive immune responses across tumor types. In HNSCC specifically, Moutafi *et al.*[16,17] have argued that PARPi-induced DNA damage increases inflammation and immune cell infiltration, "resetting" an immunologically cold tumor microenvironment, and have translated this rationale into a phase II window study of olaparib alone or with cisplatin or durvalumab; a subsequent phase II trial combining olaparib with pembrolizumab and carboplatin as first-line treatment of recurrent or metastatic HNSCC reported encouraging synergy between PARPi and anti–PD-1 therapy.[22] The present data confirm that the mechanistic substrate of this rationale—DNA damage-coupled innate immune activation—is fully operational in HSC3 and SCC25 cells, with IFNB1 induction of 8–11-fold and IFN-β secretion rising from sub-detectable to approximately 40 pg/mL upon olaparib treatment. At the same time, these findings add a critical caveat to this paradigm: this immunogenic coupling is fragile and can be decoupled by the resident microbiota, a consideration none of the aforementioned studies addressed.

The suppressive activity of intracellular *F. nucleatum* reported here resonates strongly with, and extends, a growing body of evidence that intratumoral bacteria actively sculpt immune responses in HNSCC. Silver *et al.*[15] showed that intratumoral bacteria are immunosuppressive,

promote immunotherapy resistance in HNSCC, and that antibiotic decontamination can restore treatment sensitivity. While Silver and colleagues documented the population-level impact of the intratumoral microbiome on checkpoint inhibitor outcomes, this study identifies a specific molecular locus of that suppression: the tumor cell-intrinsic cGAS–STING node. The immunomodulatory properties of *F. nucleatum* are equally well established in the colorectal cancer literature, where Kostic *et al.*[9] showed that the bacterium modulates the tumor-immune microenvironment to potentiate intestinal tumorigenesis—findings that mirror the ability of oral bacteria to promote tumorigenesis in squamous cell carcinoma mouse models[30]—and recapitulate the autoaggregation and host-cell invasion behaviors first characterized in colorectal cancer.[31] Gur *et al.*[11] demonstrated that the Fap2 adhesin engages the inhibitory receptor TIGIT on NK cells and T lymphocytes to protect tumors from immune attack, while McIlvanna *et al.*[10] and Pignatelli *et al.*[12] have reviewed these mechanisms in the oral cancer context, emphasizing Fap2/TIGIT engagement, RadD-dependent lymphocyte death, and PD-L1 induction. The present data complement these reports in two respects. First, they localize microbial immune evasion to the tumor cell-intrinsic DNA-sensing apparatus: STING agonism largely restores interferon and chemokine output in infected cells, indicating that *F. nucleatum* interferes with damage sensing or early signal transduction rather than terminal effector function. This interpretation is mechanistically consistent with recent evidence from Chauvin *et al.*[25], who showed that microbial DNA acts as a natural antagonist of the cGAS–STING pathway by competitively dampening cytosolic DNA sensing, and with the broader framework articulated by Decout *et al.*[24], in which the cGAS–STING pathway operates as a sensor of cellular damage whose activation threshold is tunable by microbial products. Second, the present data demonstrate a functional consequence at the level of immune crosstalk: conditioned-media transfer experiments showed that the PARPi-induced macrophage-priming activity of the HNSCC secretome—reflected in a 3.4-fold increase in TNF-α release—is lost when cells harbor intracellular bacteria, linking a cell-intrinsic molecular defect to a tissue-level immunological outcome. This crosstalk dimension echoes observations by Baraniya *et al.*[27], who showed that oral bacteria profoundly reprogram the transcriptional landscape of OSCC cells in co-culture, and by Dohlman *et al.*[32], who demonstrated that microbes drive transcriptional networks in a cancer type- and organ-specific manner, including in HNSCC.

The finding that bacterial colonization did not diminish olaparib-induced 8-OHdG accumulation, while profoundly blunting downstream interferon signaling, deserves particular emphasis because it clarifies the level at which the microbe intervenes. The present results are thus consistent with a model in which *F. nucleatum* leaves the drug-induced lesion burden intact but raises the activation threshold of, or actively antagonizes, cytosolic DNA sensing—precisely the scenario predicted by the microbial DNA antagonism data of Chauvin *et al.*[25] and by the damage-sensing framework of Decout *et al.*[24] **Figure 8** integrates these observations into a unified mechanistic model of the tumor cell–immune interface. In the activating limb, olaparib-induced oxidative DNA damage—quantified here as 8-OHdG accumulation in the presence of intranuclear ROS—feeds cytosolic DNA into the cGAS–STING–TBK1–IRF3 axis, and the resulting IFN-β and CXCL10 secretion primes macrophage activation, as documented in the conditioned-media transfer experiments. In the suppressive limb, intracellular *F. nucleatum* blocks this axis at the cGAS–STING level, while simultaneously elevating PD-L1 and TGF-β1 on the tumor cell surface and blunting chemokine output, thereby converting an immunostimulatory response into an immunosuppressive one. In the rescuing limb, direct STING stimulation with cGAMP or diABZI bypasses the microbial blocks and restores much of the interferon and chemokine output, although PD-L1 upregulation persists—a persistence that likely explains why STING agonism alone produced only partial functional recovery in the present experiments. This tripartite architecture is consistent with, and extends, the broader biology of how microbial products and metabolites reshape tumor cell behavior: the well-documented ability of microbiota-derived short-chain fatty acids and aromatic metabolites to modulate glycolysis, oxidative stress signaling, and epithelial differentiation in oral cancer cells[33] demonstrates how deeply microbial chemistry is embedded in tumor cell biology, and reinforces the plausibility of the central finding that microbial colonization likewise retunes the DNA damage–immune signaling axis. Reconciling these parallel observations—that microbial molecules can both elevate ROS-associated tumor cell stress and, as in the present system, attenuate ROS-coupled damage signaling—likely reflects the distinction between free metabolites and live intracellular bacteria, and constitutes an important conceptual frontier.

Several mechanistic hypotheses for the observed interference merit explicit discussion, and all three remain compatible with the data presented here. First, *F. nucleatum* may limit the cytosolic availability of the DNA ligands that activate cGAS, either through nucleases or through sequestration of damage signaling within bacterial vacuolar niches; evasion of cGAS–STING sensing is a documented strategy among diverse intracellular

pathogens.[24,25] Second, microbial metabolites—including the short-chain fatty acids that *F. nucleatum* produces abundantly—can inhibit histone deacetylases and thereby reprogram interferon-stimulated gene expression, a mechanism with established precedent in colorectal cancer and directly relevant to the ovarian cancer data of Okazawa-Sakai *et al.*[34], who associated gut microbiome composition and butyrate metabolism with PARPi efficacy in patients. However, butyrate is unlikely to be the only microbial factor involved. Other metabolites and bacterial products, including polyamines, sulfur-containing metabolites, and components that affect oxidative stress, nuclear factor kappa B signaling, interferon responses, and extracellular-vesicle communication, may also contribute to the effects of *F. nucleatum*. Recent studies have reported functional differences among *F. nucleatum* subspecies in the OSCC immune microenvironment and have shown that *F. nucleatum*-stimulated OSCC-cell exosomes can promote a pro-adhesive phenotype in lymphatic endothelial cells through the ROS/nuclear factor kappa B/intercellular adhesion molecule 1 pathway.[35,36,37] These mechanisms may also influence PARPi-induced cGAS–STING signaling, but they were not directly tested in the present study. Third, the partial suppression observed with heat-killed bacteria suggests that surface components such as lipopolysaccharide engage Toll-like receptor signaling in a manner that may feedback negatively on interferon responses, whereas the limited effect of cell-free supernatant argues against a dominant role for soluble toxins alone. These possibilities are not mutually exclusive, and dissecting their relative contributions—through nuclease-deficient bacterial mutants, targeted metabolite profiling, and chromatin immunoprecipitation of interferon-stimulated promoters—constitutes an important direction for follow-up work.

Because intracellular bacterial burden is what conditions the magnitude of microbial suppression, the vulnerability described here is concentrated in the tumor compartment: the PARPi–microbiome interaction operates most potently where high intracellular bacterial burdens coincide with activated DNA damage sensing, both hallmarks of the malignant cells themselves rather than of the surrounding epithelium—a consideration that parallels the established therapeutic window of PARPi in homologous recombination-deficient cancers.[19,20] The clinical implications of these findings are substantial when viewed against the current therapeutic landscape of HNSCC. HNSCC harbors some of the highest intratumoral bacterial burdens of any solid tumor,[3,15,38] *Fusobacterium* enrichment correlates with poorer outcomes and checkpoint inhibitor resistance,[12,39] and olaparib-based combinations are advancing through phase II trials,[17,22] complementing the checkpoint inhibitor strategies that have transformed recurrent and metastatic HNSCC management.[40] If intratumoral bacteria systematically blunt the immunogenic component of PARPi activity, as the present data suggest, three consequences follow. The efficacy of PARPi–immunotherapy combinations may vary with the patient's intratumoral microbiome composition, offering an explanation for response heterogeneity that complements the microbiome-stratified response variability documented for PD-1 blockade by Routy *et al.*[39] Microbiome-directed interventions—antibiotic decontamination as validated by Silver *et al.*[15], targeted bacteriotherapy, or metabolite modulation—may serve as rational combinatorial partners for PARPi. Finally, direct STING agonism, as suggested by the rescue experiments in which cGAMP and diABZI restored *IFNB1* induction from approximately 3-fold to 6–7-fold in infected cells, may bypass microbial suppression of damage sensing.[41,42] Prospective biomarker studies stratifying PARPi trial participants by intratumoral bacterial load—building on the prognostic intracellular bacterial associations reported by Zang *et al.*[14] and the HPV-dependent oncobacteria abundance patterns described by Kerr *et al.*[42]—would directly test these predictions.

This study has limitations. The model system is *in vitro* and relies on two HNSCC cell lines; microbial effects may differ in magnitude and direction in primary cultures, organoids, or *in vivo*, where stromal and immune compartments add further complexity. Whole-transcriptome profiling was not performed, which would have revealed additional microbial effects beyond the cGAS–STING axis, and the functional immune readout was limited to monocyte-derived macrophage activation rather than the full complement of innate and adaptive effectors. The bacterial colonization protocol models acute infection rather than the chronic, biofilm-like state present in patient tumors, and intracellular bacteria were not formally distinguished from tightly adherent bacteria beyond gentamicin protection. Finally, the numerical results reported here derive from controlled *in vitro* experiments and require validation in independent laboratories and in patient-derived material before clinical translation.

5. Conclusion

In conclusion, intracellular *F. nucleatum* dampens PARPi-induced cGAS–STING innate immune signaling in HNSCC cells and shifts the tumor secretome toward an immunosuppressive phenotype characterized by elevated PD-L1 and TGF-β1, reduced type I interferon and CXCL10, and weakened macrophage activation. These findings identify the intratumoral oral microbiome as a

modulator of the immunogenic pharmacology of PARPi and provide a mechanistic rationale for combining PARP inhibition with STING agonism or microbiome-directed strategies in HNSCC.

Acknowledgments

None.

Funding

None.

Conflict of interest

The author declares no competing interests.

Author contributions

This is a single-authored article.

Ethics approval and consent to participate

Not applicable.

Consent for publication

Not applicable.

Availability of data

Data are available from the corresponding author upon reasonable request.

References

1. Warnakulasuriya S. Global epidemiology of oral and oropharyngeal cancer. *Oral Oncol.* 2009;45(4-5);309–316.

   doi: 10.1016/j.oraloncology.2008.06.002

2. Chen JW, Wu JH, Chiang WF, Chen YL, Wu WS, Wu LW. Taxonomic and Functional Dysregulation in Salivary Microbiomes During Oral Carcinogenesis. *Front Cell Infect Microbiol.* 2021;11:663068.

   doi: 10.3389/fcimb.2021.663068

3. Banerjee S, Tian T, Wei Z, *et al.* Microbial signatures associated with oropharyngeal and oral squamous cell carcinomas. *Sci Rep.* 2017;7(1):4036.

   doi: 10.1038/s41598-017-03466-6.

4. Wang S, Tan X, Cheng J, *et al.* Oral microbiome and its relationship with oral cancer. *J Cancer Res Ther.* 2024;20(4):1141-1149.

   doi: 10.4103/jcrt.jcrt_44_24.

5. Golusińska-Kardach E, Yadav H, Jain S, Masternak MM, Golusiński W. The Oral Microbiome and Head and Neck Cancer: A Narrative Review. *Cancers.* 2025;17(17):2736.

   doi: 10.3390/cancers17172736

6. Hayes RB, Ahn J, Fan X, *et al.* Association of oral microbiome with risk for incident head and neck squamous cell cancer. *JAMA Oncol.* 2018;4(3):358-365.

   doi: 10.1001/jamaoncol.2017.4777.

7. Brennan CA, Garrett WS. Fusobacterium nucleatum—symbiont, opportunist and oncobacterium. *Nat Rev Microbiol.* 2019;17(3):156-166.

   doi: 10.1038/s41579-018-0129-6

8. Feres M, Teles F, Teles R, Figueiredo LC, Faveri M. The subgingival periodontal microbiota of the aging mouth. *Periodontol* 2000. 2016;72(1):30-53.

   doi: 10.1111/prd.12136

9. Kostic AD, Chun E, Robertson L, *et al.* Fusobacterium nucleatum potentiates intestinal tumorigenesis and modulates the tumor-immune microenvironment. *Cell Host Microbe.* 2013;14(2):207-215.

   doi: 10.1016/j.chom.2013.07.007

10. McIlvanna E, Linden GJ, Craig SG, Lundy FT, James JA. Fusobacterium nucleatum and oral cancer: a critical review. *BMC Cancer.* 2021;21(1):1212.

    doi: 10.1186/s12885-021-08903-4.

11. Gur C, Ibrahim Y, Isaacson B, *et al.* Binding of the Fap2 protein of Fusobacterium nucleatum to human inhibitory receptor TIGIT protects tumors from immune cell attack. *Immunity.* 2015;42(2):344-355.

    doi: 10.1016/j.immuni.2015.01.010

12. Pignatelli P, Nuccio F, Piattelli A, Curia MC. The Role of Fusobacterium nucleatum in Oral and Colorectal Carcinogenesis. *Microorganisms.* 2023;11(9):2358.

    doi: 10.3390/microorganisms11092358

13. Fu A, Yao B, Dong T, *et al.* Tumor-resident intracellular microbiota promotes metastatic colonization in breast cancer. *Cell.* 2022;185(8):1356-1372.e26.

    doi: 10.1016/j.cell.2022.02.027

14. Zang X, Li X, Sun R, *et al.* Intratumoral microbiota drive immune evasion and disease progression in oral squamous cell carcinoma. *BDJ Open.* 2025;11(1):89.

    doi: 10.1038/s41405-025-00385-x

15. Silver NL, Dai J, Kerr TD, *et al.* Intratumoral bacteria are immunosuppressive and promote immunotherapy resistance in head and neck squamous cell carcinoma. *Nat Cancer.* 2026;7:80-97.

    doi: 10.1038/s43018-025-01067-1

16. Moutafi M, Economopoulou P, Rimm D, Psyrri A. PARP inhibitors in head and neck cancer: molecular mechanisms, preclinical and clinical data. *Oral Oncol.* 2021;117:105292.

    doi: 10.1016/j.oraloncology.2021.105292

17. Moutafi M, Koliou GA, Papaxoinis G, *et al*. Phase II window study of olaparib alone or with cisplatin or durvalumab in operable head and neck cancer. *Cancer Res Commun.* 2023;3(8):1514-1523.

doi: 10.1158/2767-9764.CRC-23-0051

18. Murai J, Huang SY, Das BB, *et al*. Trapping of PARP1 and PARP2 by clinical PARP inhibitors. *Cancer Res.* 2012;72(21):5588-5599.

doi: 10.1158/0008-5472.CAN-12-2753

19. Pantelidou C, Sonzogni O, De Oliveria Taveira M, *et al*. PARP inhibitor efficacy depends on CD8+ T-cell recruitment via intratumoral STING pathway activation in BRCA-deficient models of triple-negative breast cancer. *Cancer Discov.* 2019;9(6):722-737.

doi: 10.1158/2159-8290.CD-18-1218

20. Shen J, Zhao W, Ju Z, *et al*. PARPi triggers the STING-dependent immune response and enhances the therapeutic efficacy of immune checkpoint blockade independent of BRCAness. *Cancer Res.* 2019;79(2):311-319.

doi: 10.1158/0008-5472.CAN-18-1003

21. Ding L, Kim HJ, Wang Q, *et al*. PARP inhibition elicits STING-dependent antitumor immunity in Brca1-deficient ovarian cancer. *Cell Rep.* 2018;25(11):2972-2980.e5.

doi: 10.1016/j.celrep.2018.11.054

22. Adkins D, Ley JC, Liu J, Oppelt P. Olaparib, pembrolizumab, and carboplatin as first-line treatment of recurrent or metastatic head and neck squamous cell carcinoma: a phase II trial. *JCO Oncol Adv.* 2025;2(1).

doi: 10.1200/OA-25-00049

23. Yao Y, Zhu Y, Chen K, *et al*. Microbiota in cancer: current understandings and future perspectives. *Signal Transduct Target Ther.* 2026;11(1):39.

doi: 10.1038/s41392-025-02335-3

24. Decout A, Katz JD, Venkatraman S, Ablasser A. The cGAS-STING pathway as a therapeutic target in inflammatory diseases. *Nat Rev Immunol.* 2021;21(9):548-569.

doi: 10.1038/s41577-021-00524-z

25. Chauvin SD, Stinson WA, Platt DJ, Poddar S, Miner JJ. Regulation of cGAS and STING signaling during inflammation and infection. *J Biol Chem.* 2023;299(7):104866.

doi: 10.1016/j.jbc.2023.104866

26. Taghavi Pourianazar N. ROS-induced DNA damage enhances sensitivity to PARP inhibition in HSC3 and SCC25 head and neck squamous cell carcinoma cell lines. *Curr Issues Mol Biol.* 2026;48(7):692.

doi: 10.3390/cimb48070692

27. Baraniya D, Chitrala KN, Al-Hebshi NN. Global transcriptional response of oral squamous cell carcinoma cell lines to health-associated oral bacteria: an in vitro study. *J Oral Microbiol.* 2022;14(1):2073866.

doi: 10.1080/20002297.2022.2073866

28. Lee EK, Konstantinopoulos PA. PARP inhibition and immune modulation: scientific rationale and perspectives for the treatment of gynecologic cancers. *Ther Adv Med Oncol.* 2020;12:1-16.

doi: 10.1177/1758835920944116

29. Zitvogel L, Galluzzi L, Kepp O, Smyth MJ, Kroemer G. Type I interferons in anticancer immunity. *Nat Rev Immunol.* 2015;15(7):405-414.

doi: 10.1038/nri3845

30. Stashenko P, Yost S, Choi Y, *et al*. The oral mouse microbiome promotes tumorigenesis in oral squamous cell carcinoma. *mSystems.* 2019;4(4).

doi: 10.1128/mSystems.00323-19

31. Udayasuryan B, Zhou Z, Ahmad RN, *et al*. Fusobacterium nucleatum infection modulates the transcriptome and epigenome of HCT116 colorectal cancer cells in an oxygen-dependent manner. *Commun Biol.* 2024;7(1):551.

doi: 10.1038/s42003-024-06201-w

32. Dohlman AB, Arguijo Mendoza D, Ding S, *et al*. The cancer microbiome atlas: a pan-cancer comparative analysis to distinguish tissue-resident microbiota from contaminants. *Cell Host Microbe.* 2021;29(2):281-298.e5.

doi: 10.1016/j.chom.2020.12.001

33. Zhao K, Cui S, Wang N, et al. The cGAS-STING pathway and mitochondrial metabolism: from mechanistic insights to therapeutic potential in tumor. J Transl Med. 2026;24(1):294.

doi: 10.1186/s12967-026-07748-4

34. Okazawa-Sakai M, Sakai SA, Hyodo I, *et al*. Gut microbiome associated with PARP inhibitor efficacy in patients with ovarian cancer. *J Gynecol Oncol.* 2025;36(3).

doi: 10.3802/jgo.2025.36.e38

35. Yang X, Zhang S, Ning T, Wu J. Fusobacterium nucleatum in health and disease. *MedComm.* 2025;6(11).

doi: 10.1002/mco2.70465

36. Yano M, Kamiya T, Yamamoto Y, *et al*. Functional heterogeneity of Fusobacterium nucleatum subspecies in the immune microenvironment of oral squamous cell carcinoma. *Microorganisms.* 2026;14(9):2067.

doi: 10.3390/microorganisms14092067

37. Wei L, He Q, Gao H, Li W, Sun T, Feng Q. Fusobacterium nucleatum-stimulated OSCC cell-derived exosomes induce a pro-adhesive phenotype in lymphatic endothelial cells via the ROS/NF-κB/ICAM1 axis. *Microorganisms.* 2026;14(9):1965.

doi: 10.3390/microorganisms14091965

38. Qiao H, Li H, Wen X, Tan X, Yang C, Liu N. Multi-omics integration reveals the crucial role of Fusobacterium in the inflammatory immune microenvironment in head and neck squamous cell carcinoma. *Microbiol Spectr.* 2022;10(4):e01068-22.

doi: 10.1128/spectrum.01068-22

39. Routy B, Le Chatelier E, Derosa L, *et al*. Gut microbiome influences efficacy of PD-1-based immunotherapy against epithelial tumors. *Science.* 2018;359(6371):91-97.

doi: 10.1126/science.aan3706

40. Harrington KJ, Ferris RL, Blumenschein G, *et al*. Nivolumab versus standard, single-agent therapy of investigator's choice in recurrent or metastatic squamous cell carcinoma of the head and neck (CheckMate 141): health-related quality-of-life results from a randomised, phase 3 trial. *Lancet Oncol.* 2017;18(8):1104-1115.

doi: 10.1016/S1470-2045(17)30421-7

41. Corrales L, McWhirter SM, Dubensky TW Jr, Gajewski TF. The host STING pathway at the interface of cancer and immunity. *J Clin Invest.* 2016;126(7):2404-2411.

doi: 10.1172/JCI86892

42. Kerr TD, Silver NL, Duggal R, *et al*. HPV status impacts oncobacteria abundance and prognostic relevance in head and neck squamous cell carcinoma. *Oncogene.* 2025;44(26):2217-2223.

doi: 10.1038/s41388-025-03463-4